

DNA-Mediated Electron Transfer across Synthetic T:A·T Triplex Structures**

Frederick D. Lewis,* Yansheng Wu, Ryan T. Hayes, and Michael R. Wasielewski*

Oligonucleotides which contain three sequences capable of triplex formation, and which are connected with appropriate linkers, can fold into intramolecular triplex structures.^[1] Both natural and synthetic linkers have been used to assemble intramolecular T:A·T triplexes in which poly(T:A) forms a normal Watson–Crick duplex and the third strand (polyT) is parallel to the polyA sequence and associated by Hoogsteen hydrogen bonding (Figure 1a,b).^[2–4] The conformation of intermolecular poly(T:A·T) triplexes is similar to that of duplex B-DNA with a π -stacking distance of 3.3 Å and a helical pitch of 28°. We report here the preparation of the donor–acceptor intramolecular triplex DNA structures **1–5** which possess a stilbenedicarboxamide derivative (**Sa**) as an electron-acceptor linker and a stilbenediether derivative (**Sd**) as an electron-donor linker (Figure 1c,d). The two chromophores undergo intramolecular, photoinduced electron transfer across the π -stacked triplets by single-step tunneling (for **1–4**) and multistep hopping (for **5**) pathways.

The conjugates **1–5** were prepared by conventional phosphoramidite methods as previously described for the preparation of **Sa**- and **Sd**-linked hairpins.^[5,6] The 3'-3' linkages between the Watson–Crick T:A hairpin sequence and the Hoogsteen-bound polyT were formed by 5' solid-phase oligonucleotide synthesis. The absorption spectra of conjugates **1–5** consist of a broad, long wavelength band with a maximum at 340 nm that is attributed to the overlapping absorptions of the **Sa** and **Sd** chromophores and a band at 260 nm attributed to absorption of these chromophores and the nucleobases.^[7] The thermal dissociation profiles are independent of concentration and display melting transitions at between 60–71 °C, which are attributed to melting of the **Sd**-capped **Sa**-linked Watson–Crick duplex, and premelting behavior at lower temperatures, which is attributed to melting of the Hoogsteen base pairs.^[8]

The fluorescence spectra of the conjugates **1–5** are similar to those of **Sa**-linked hairpins such as **6**.^[5] The **Sa**-linked poly(T:A) hairpins are strongly fluorescent, whereas the **Sd**-linked hairpins are very weakly fluorescent, as a consequence of quenching of the singlet form of **Sd** by neighboring thymine.^[6] The fluorescence intensity of **1–5** is strongest when

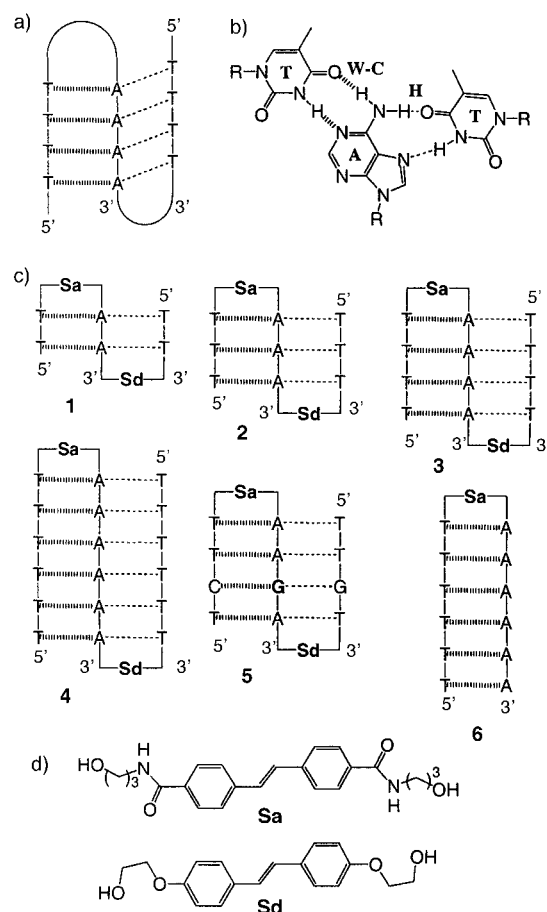


Figure 1. a) Structure of an intramolecular antiparallel DNA triplex with Watson–Crick (W–C |||||) and Hoogsteen (H ----) hydrogen bonding; b) structure of the T:A·T canonical triplet; c) structure of intramolecular triplexes **1–5** and hairpin **6**; d) structures of the **Sa** and **Sd** linkers.

excited in the red edge of the 340 nm absorption band, where **Sa** absorbs more strongly than **Sd**. The value of Φ_f for conjugates **1–4** decreases as the number of T:A·T steps separating the **Sa** and **Sd** chromophores decreases (Table 1),^[7] in accord with an electron-transfer mechanism for fluorescence quenching of **Sa** by **Sd**. The free energy of the photochemical electron transfer process can be estimated using Weller's equation [$\Delta G_{et} = -(E_s + E_{rdn}) + E_{ox}$], using the **Sa** singlet excitation energy ($E_s = 3.35$ V) and ground-state reduction potential $E_{rdn} = -1.91$ V (vs. SCE in DMF solution) and the **Sd** oxidation potential ($E_{ox} = 0.92$ V).^[5,6] The resulting value of $\Delta G_{et} = -0.52$ eV shows that this reaction is more exergonic than quenching of **Sa** by G ($\Delta G_{et} = -0.20$ eV).

Normalized time-resolved transient absorption spectra of conjugate **1** are shown in Figure 2. The spectrum observed 5 ps after excitation at 360 nm (absorbed predominantly by **Sa**) is assigned to $^1\text{Sa}^*$ (575 nm maximum and 625 nm shoulder). At longer delay times the shoulder at 625 nm disappears and maxima are observed at 525 and 575 nm, assigned to Sd^{+} and Sa^- , respectively.^[5] The 575 nm decays of **1–5** display fast (ps to ns) and slow (ns to μ s) components, which are assigned to decay of $^1\text{Sa}^*$ and Sa^- , respectively (Table 1). The 525 nm decay of **1** displays both rising and falling components with time constants similar to those for the two 575 nm components and assigned to the formation and

[*] Prof. F. D. Lewis, Prof. M. R. Wasielewski, Dr. Y. Wu, R. T. Hayes
Department of Chemistry
Northwestern University
Evanston, IL 60208-3113 (USA)
Fax: (+1) 847-467-2184
E-mail: lewis@chem.northwestern.edu
wasielew@chem.northwestern.edu

[**] This research is supported by grants from the Division of Chemical Sciences, Office of Basic Energy Sciences, U.S. Department of Energy under contracts DE-FG02-96ER14684 (F.D.L.) and by DE-FG02-99ER14999 (M.R.W.).

Supporting information for this article is available on the WWW under <http://www.angewandte.org> or from the author.

Table 1. Fluorescence quantum yields and transient decay times for conjugates 1–6.^[a]

Conjugate	$\Phi_f^{[b]}$	τ_s , ps ([%]) ^[c,d]	$k_{cs} \times 10^{-9}$ [s ⁻¹] ^[e]	τ_{575} [ns] ([%]) ^[d,f]	τ_{525} [ns] ^[g]	$k_{cr} \times 10^{-7}$ [s ⁻¹] ^[h]
1	0.06	75 (30)	13	8.4 (70)	8.2 ^[i]	12
2	0.18	280 (49)	3.1	127 (51)	145	7.4
3	0.32	540 (55)	1.3	5800 (45)	8200	0.14
4	0.31	1800 (100)	0.5	^[j]	^[j]	
5	0.08	141 (37)	6.6	800 (25)		0.15 ^k
6	0.38	2000 (100)		6700 (38)	^[j]	

[a] Data for approximately 10⁻⁶ M solutions in standard buffer (0.1 M NaCl, 10 mM sodium phosphate, pH 7.2). [b] Fluorescence quantum yields determined by comparison to quinine sulfate. Limits of error for multiple detection $\pm 10\%$. [c] Decay of the singlet state determined at 575 nm, estimated error $\pm 10\%$ of the reported value. [d] Amplitudes for 575 nm decay in parentheses. [e] Rate constant for charge separation, $k_{cs} = \tau_{obs}^{-1} - \tau_6^{-1}$. [f] Decay component assigned to charge recombination of **Sa**^{-•}. [g] Decay component assigned to charge recombination of **Sd**^{+•}. [h] Rate constant for charge recombination, $k_{cr} = \tau_{obs}^{-1}$. Average of 575 and 525 nm values where available. [i] Rising component with $\tau = 94$ ps also resolved. [j] No long-lived transient resolved. [k] Estimated from the long-lived 575 nm decay component.

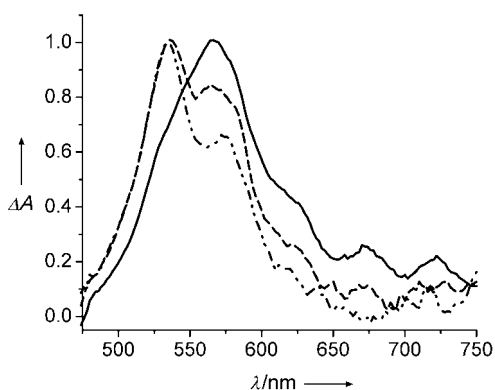
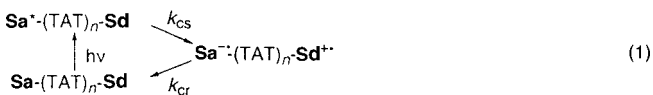


Figure 2. Normalized transient absorption spectra for conjugate 1 obtained at delay times of 5 ps (—), 100 ps (---), and 1 ns (•••) following excitation at 360 nm with a 0.13 ps laser pulse.

decay of **Sd**^{+•},^[6] respectively. The formation and decay of **Sa**^{-•} and **Sd**^{+•} is attributed to charge separation and charge recombination (k_{cr} and k_{cs} , respectively) through single-step electron tunneling across a bridge consisting of T:A:T triplet steps [Eq. (1)].



Plots of $\ln(k_{cr})$ and $\ln(k_{cs})$ versus the donor–acceptor distance (R_{DA}) for conjugates 1–4 are shown in Figure 3, along with data for quenching of **Sa** by G in **Sa**-linked hairpin molecules containing a single C:G base pair.^[5] The slopes of these plots provide values of β [$k_{cs} = A \exp(-R_{DA}\beta)$], where R_{DA} is the distance between the donor and acceptor. The value of β obtained for triplex charge separation is smaller than that for duplex hairpin charge separation ($\beta = 0.39$ vs. 0.64 \AA^{-1}), whereas the values of β for charge recombination are similar for the triplex and duplex ($\beta = 1.0$ vs. 0.94 \AA^{-1}).^[9] The magnitude of β is determined by the energy gap between

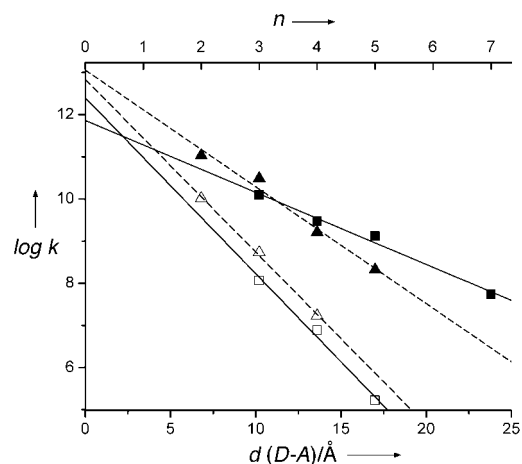


Figure 3. Distance dependence (n is the number of base triplets separating the donor and acceptor) of the rate constants obtained from transient absorption data for charge separation (filled symbols) and charge recombination (open symbols) from triplex (squares) and hairpin (triangles) conjugates.

the donor and bridge states (ΔE eV) and the time after mixing elements (t_{mn}) between bridge states ($\beta = (2R_0) \ln |\Delta E/t_{mn}|$).^[10,11] The shorter distance between steps in triplex versus duplex DNA (3.3 vs. 3.4 \AA) should result in increased mixing. In addition, increased hydrogen bonding in the triplex versus duplex should lower the oxidation potential of adenine in the bridging T:A:T triples.^[12] Both factors could contribute to the decrease in β for triplex versus duplex charge separation. However, a decrease in the energy of the charge-separated state for **Sa**^{-•}/**Sd**^{+•} versus **Sa**^{-•}/**G**^{+•} may compensate for increased mixing in the triplex, resulting in similar values of β for charge recombination in the triplex and duplex systems.

Conjugate 5 possesses a C:G:G triplet positioned between the **Sd** and **Sa** linkers. The value of k_{cs} obtained for 5 from the 575 nm ps decay is larger than that for 3, in accord with primary electron transfer from G to **Sa**^{*}. The curve of decay of the radical ions is best fit by a biexponential function with decay times of 0.8 and 6.7 μs , which is attributed to charge recombination of the primary **Sa**^{-•}/**G**^{+•} radical ion pair and of the **Sa**^{-•}/**Sd**^{+•} secondary radical-ion pair formed by exergonic hole transport from **G**^{+•} to **Sd**.^[13–15] The long decay time for 5 is similar to that for an **Sa**-linked hairpin with an **Sa**-AAGAZA (**Z** = deazaguanine) hole-hopping sequence. The oxidation potentials of **Sd** and **Z** are similar and thus both systems will have similar values of ΔG_{cr} .

In summary, we have, for the first time, characterized both the radical anion and radical cation products of photoinduced electron transfer mediated by DNA. Long-range single-step electron transfer is rapid for triplex than duplex DNA, plausibly because of the shorter π -stacking distance and lower energy of the T:A:T versus T:A bridging states. The value of $\beta = 0.39 \text{ \AA}^{-1}$ for charge separation is the smallest value yet determined from the direct measurement of distance-dependent dynamics. In the case of conjugate 5, formation of a long-lived charge-separated state occurs by a hole-transport mechanism in which G and **Sd** serve as the primary and secondary hole acceptors, respectively. Introduction of multiple hopping sites should facilitate efficient charge transfer between **Sa** and **Sd** linkers across long triplex sequences.

Supporting Information available: Ultraviolet absorption and fluorescence spectra of the conjugates and representative transient absorption spectra and transient decays.

Received: May 7, 2002 [Z19252]

- [1] E. Wang, J. Feigon in *Nucleic Acid Structure* (Ed.: S. Neidle), Oxford, Oxford, **1999**.
- [2] M. Tarköy, A. K. Phillips, P. Schultze, J. Feigon, *Biochemistry* **1998**, *37*, 5810.
- [3] M. Salunkhe, T. Wu, R. L. Letsinger, *J. Am. Chem. Soc.* **1992**, *114*, 8768.
- [4] R. Macaya, E. Wang, P. Schultze, V. Sklenár, J. Feigon, *J. Mol. Biol.* **1992**, *225*, 755.
- [5] F. D. Lewis, T. Wu, X. Liu, R. L. Letsinger, S. R. Greenfield, S. E. Miller, M. R. Wasielewski, *J. Am. Chem. Soc.* **2000**, *122*, 2889.
- [6] F. D. Lewis, X. Liu, Y. Wu, S. E. Miller, M. R. Wasielewski, R. L. Letsinger, R. Sanishvili, A. Joachimiak, V. Tereshko, M. Egli, *J. Am. Chem. Soc.* **1999**, *121*, 9905.
- [7] Data provided as Supporting Information.
- [8] Detailed information concerning the synthesis and characterization of triplex-forming conjugates will be reported separately. The UV thermal dissociation and circular dichroism spectra of **2–5** are consistent with the assignment of triplex structures. In the case of **1**, the structure may be an end-capped hairpin rather than a triplex.
- [9] Values of k_{es} can also be calculated from fluorescence quantum-yield data. However, these values are considered to be less reliable than those obtained from transient decay measurements (Table 1), because imperfectly folded conformations of the conjugates should have high fluorescence quantum yields.
- [10] F. C. Grozema, Y. A. Berlin, L. D. A. Siebbeles, *J. Am. Chem. Soc.* **2000**, *122*, 10903.
- [11] G. S. M. Tong, I. V. Kurnikov, D. N. Beratan, *J. Phys. Chem. B* **2002**, *106*, 2381.
- [12] K. Kawai, Y. Wata, N. Ichinose, T. Majima, *Angew. Chem.* **2000**, *112*, 4497; *Angew. Chem. Int. Ed.* **2000**, *39*, 4327.
- [13] F. D. Lewis, X. Liu, J. Liu, S. E. Miller, R. T. Hayes, M. R. Wasielewski, *Nature* **2000**, *406*, 51.
- [14] Kan and Schuster^[15] have investigated strand cleavage resulting from hole migration in triplex DNA.
- [15] Y. Kan, G. B. Schuster, *J. Am. Chem. Soc.* **1999**, *121*, 11607.

Electrocatalytic O₂ Reduction by Synthetic Analogues of the Heme/Cu Site of Cytochrome Oxidase Incorporated in a Lipid Film**

James P. Collman* and Roman Boulatov

Over 95% of dioxygen consumed by an aerobe is used in respiration,^[1] whereby O₂ is reduced by four electrons (4e) to two molecules of H₂O. In most aerobes the reduction occurs at a heterodimetallic Fe/Cu site (Figure 1A) of membrane-bound heme/Cu terminal oxidases (cytochrome c or ubiquinol

[*] Prof. J. P. Collman, R. Boulatov
Department of Chemistry
Stanford University
Stanford CA 94305 (USA)
Fax: (+1) 650-7250259
E-mail: jpc@stanford.edu

** This work was supported by the NIH and a Stanford Graduate Fellowship. We thank Dr. C. J. Sunderland for synthesis of the catalysts and Dr. I. M. Shiryaeva for helpful discussions.

Supporting information for this article is available on the WWW under <http://www.angewandte.org> or from the author.

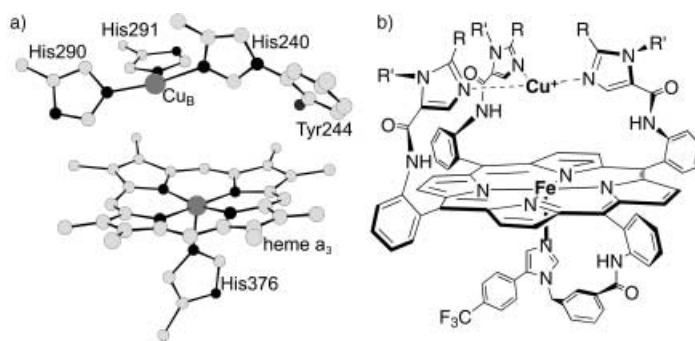
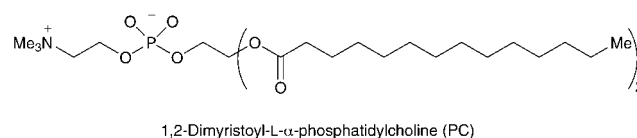


Figure 1. A) The heme/Cu site of bovine cytochrome oxidase;^[5] the C atoms are light gray and the N and O atoms are black. B) The catalysts in the reduced form without probable exogenous ligands^[6] (the NH series: R = Pr, R' = H; the NMe series: R = H, R' = CH₃).

oxidases).^[2,3] Coupling of this exergonic reaction to proton translocation against the electrochemical transmembrane gradient^[2,4] maintains the proton-motive force that drives ATP synthesis.

The O₂-reducing heme/Cu site has long been a target for biomimetic chemists.^[7] A number of synthetic Fe porphyrins with various degrees of structural similarity to the heme/Cu site when adsorbed on a graphite electrode catalyze the electrochemical 4e reduction of O₂, although rarely at physiological potentials (namely those of cytochrome c and ubiquinol). Electrocatalytic O₂ reduction is the only known method to probe the reactivity of synthetic heme/Cu analogues under catalytic and biologically relevant conditions. This technique is conceptually similar, and in some respects superior, to spectrophotometric and polarographic assays traditionally used to quantify the activity of cytochrome oxidase.^[8] Previously, biomimetic O₂ reduction have been probed only by electrode-adsorbed heme/Cu mimics. However, studies of adsorbed heme/Cu analogues, while experimentally simple, limits the potential of such systems to unravel the structure/function relationship within this enzymatic site, and thus to contribute to understanding the enzyme. Firstly, cytochrome oxidase reduces O₂ under diffusion-limited electron delivery, whereas the electron-transfer rate to an electrode-adsorbed catalyst usually far exceeds the catalytic turnover frequency (TOF). Secondly, the high concentration of redox sites in films of adsorbed catalysts creates an environment which both differs notably from that of a protein matrix and depends strongly on the overall redox state of the film.^[6b]

Herein we report on electrocatalytic O₂ reduction by a series of synthetic heme/Cu analogues (Figure 1B) incorporated into a matrix of 1,2-dimyristoyl-L- α -phosphatidylcholine (PC), which is a major constituent of mitochondrial mem-



branes. Among the known synthetic porphyrins, those employed in the present study most faithfully mimic the heme/Cu site.^[6] High dilution of the redox centers by, and relatively